Cell Migration and Invasion



# Automated Label-Free Method for Measuring Cell Migration in Real-Time with the Oris Pro Assay

#### **Authors**

Joe Clayton, Peter Brescia, and Peter Banks Agilent Technologies, Inc.

## **Abstract**

Cell migration is dependent on complex environmental signaling events and induced structural changes to the cytoskeleton. Multicellular organisms rely on cell migration for a vast array of biological processes, including embryonic development, immune responses, wound healing, and cancer metastasis. This application note demonstrates an automated kinetic imaging-based approach to investigating cell migration. This convenient label-free method enables robust analysis of cell migration in 96- or 384-well microplates for high-throughput applications.

## Introduction

Cell migration, whereby cells move from one location to another in the body, is a complex response to biochemical and mechanical interactions in the environment that is roughly encapsulated as leading edge protrusion, substratum adhesion, retraction of the rear, and de-adhesion. In response to normal cell signaling, migration is critical to a vast array of biological processes such as embryonic development, immune response, and wound healing; however, when the highly regulated network of signals is disrupted, cell migration is complicit in disease states ranging from metastasized cancers to multiple sclerosis, neurodevelopmental disorders, and more. <sup>2,3,4</sup>

Cell exclusion zone, or wound healing, assays are commonly employed in cell migration studies to screen for potential cytotoxicity in test molecules and develop novel therapies to aid wound healing abilities and control metastatic actions. In these assays, cells are seeded onto a surface that includes a barrier, thus creating a cell-free zone. Once the cells reach confluence, the barrier is removed, and cell motility into the cell-free zone is measured. Kinetic imaging enables precise tracking of cell movement over time, and label-free methods eliminate risk of potentially altered cell activity due to the presence of fluorescent probes.

## Materials and methods

#### Materials

#### Cells and reagents

HT-1080 fibrosarcoma cells (part number CCL-121) were obtained from ATCC (Manassas, VA). Human neonatal dermal fibroblasts (part number cAP-0008RFP) were obtained from Angio-Proteomie (Boston, MA). Oris Pro 96-well plates with BCG wells coated with Collagen I (part number PROCMACC5) and Oris Pro 384-well plates with BCG wells coated with Collagen I (part number PRO384CMACC5) were generously donated by Platypus Technologies. Advanced DMEM (part number 12491-015), fetal bovine serum (part number 10437-036), and penicillin-streptomycinglutamine (100x) (part number 10378-016) were purchased from Thermo Fisher Scientific (Waltham, MA). Cytochalasin D (part number 1233) was purchased from Bio-Techne Corporation (Minneapolis, MN).

#### Agilent BioTek Cytation 5 cell imaging multimode reader

Cytation 5 is a modular automated digital microscope combined with a multimode microplate reader. The microscopy module provides up to 60x magnification in fluorescence, brightfield, color brightfield, high contrast brightfield, and phase contrast. Cytation 5 supports live-cell assays, with temperature control to 65 °C, CO<sub>2</sub>/O<sub>2</sub> gas control, shaking, and dual injectors for kinetic assays. Agilent BioTek Gen5 microplate reader and imager software, automates image capture, processing, and analysis. Cytation 5 was used to kinetically monitor cell migration activity over the incubation period.

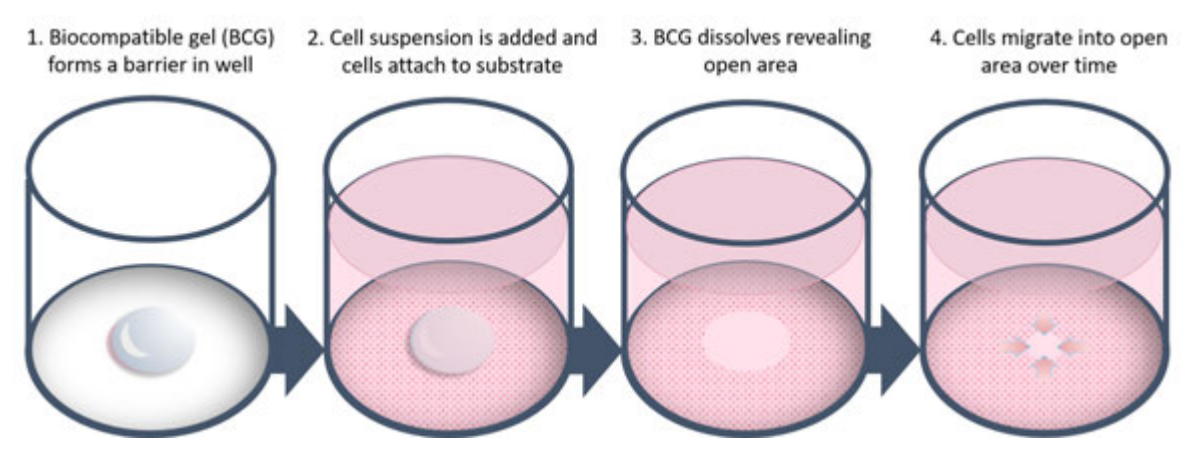


Figure 1. Oris Pro cell migration assay overview.

#### Agilent BioTek BioSpa 8 automated incubator

The BioSpa 8 automated incubator links Agilent BioTek readers or imagers together with Agilent BioTek washers and dispensers for full workflow automation of up to eight microplates. Temperature,  $CO_2/O_2$ , and humidity levels were controlled and monitored through the Agilent BioTek BioSpa software to maintain an ideal environment for cell cultures during all experimental stages. Test plates were incubated in the BioSpa to maintain proper atmospheric conditions throughout the experimental protocol and automatically transferred to the Cytation 5 every hour for high contrast brightfield imaging.

#### Agilent BioTek MultiFo FX multimode dispenser

The MultiFlo FX is a modular, upgradable reagent dispenser with as many as two peri-pumps (8 tube dispensers), two syringe pump dispensers and a strip washer. The syringe and washer manifolds can be configured for plate densities from 6- to 384-well. The MultiFlo FX was used for all aspirate and dispense steps.

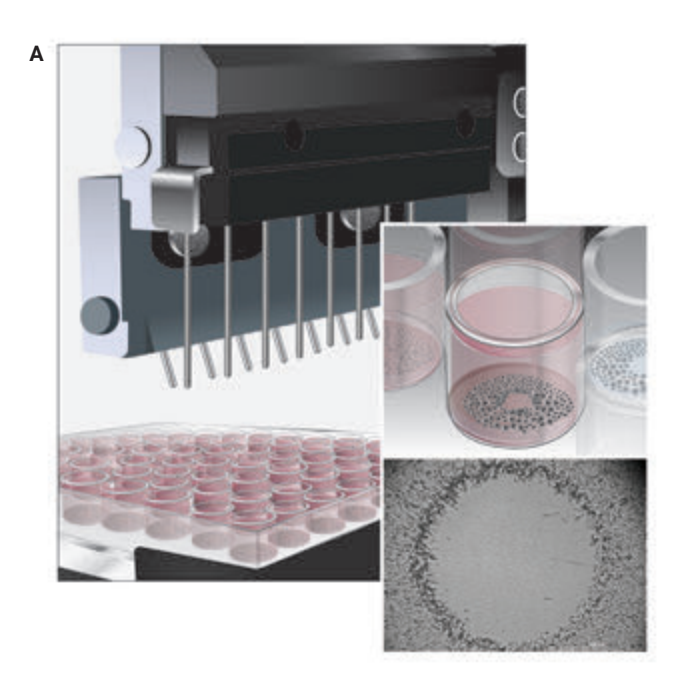
## **Methods**

#### Cell migration assay preparation

Using the MultiFlo FX, 100  $\mu$ L of prepared HT-1080 and fibroblast cell suspensions were separately added to wells of an Oris Pro 96-well plate at concentrations of 30,000 and 20,000 cells/well, respectively. The process was repeated with Oris Pro 384-well plates, dispensing HT-1080 cells and fibroblasts at concentrations of 10,000 and 7,000 cells/well, respectively, in a 20  $\mu$ L volume. The plates were briefly centrifuged to settle the cells onto the well bottom, and the plates were then incubated at room temperature for 20 minutes to allow cells to fully attach to the substrate, during which time the BCG dissolved and exposed the cell-free zone.

The process was also repeated using HT-1080 cells at a concentration of 30,000 cells/well and Oris cell migration assay stoppers in 96-well format. The stoppers were manually removed after the incubation step.

Three media aspirate/dispense cycles were performed on the assay plates to remove any excess cells that collected along the rim of the cell-free zone (Figure 2) to ensure accuracy and reproducibility of results. Eight serial titrations of cytochalasin D ranging from 1 to 0  $\mu$ M were created and dispensed in a volume of 100  $\mu$ L or 20  $\mu$ L into the 96- or 384-well microplates, respectively.



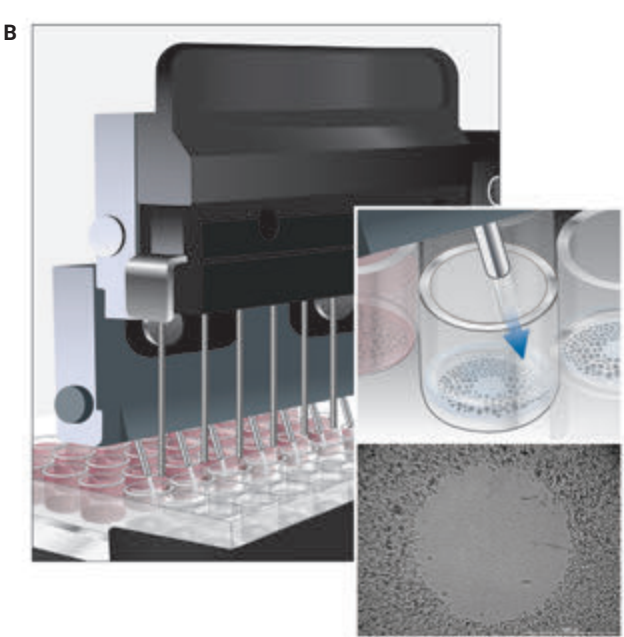


**Figure 2.** The Agilent BioTek MultiFlo FX multimode dispenser was used to remove excess cells that collected around the rim of the open area in the microplate wells after the BCG dissolved. (A) Microplate well prior to washing steps. (B) Microplate well after washing steps.

#### Kinetic live-cell imaging workflow

The Oris plates were then loaded into the BioSpa 8 automated incubator, with atmospheric conditions previously set to 37 °C, 5%  $\rm CO_2$ , and 80% humidity. The BioSpa 8 software was programmed such that the plates were automatically transferred to the Cytation 5 for high contrast brightfield imaging of each test well every hour over the experimental procedure using the 2.5x objective for the 96-well plate, and the 4x objective for the 384-well plate. Image analysis settings were automatically applied, generating quantitative migration results in real time.

#### Results and discussion

#### Automated image analysis of cell migration

The ability to automatically capture images to monitor and analyze uninhibited HT-1080 cell migration in the Oris Pro cell migration assay was initially examined. Using images captured at various time points (Figure 3A), Gen5 software in Cytation 5 automatically placed yellow object masks around cell-containing areas (Figure 3B) using predefined cellular analysis criteria. The percent closure, noted as open area relative to starting open area, was then automatically calculated and reported. The cell-free zone achieved 94% closure in approximately 12 hours.

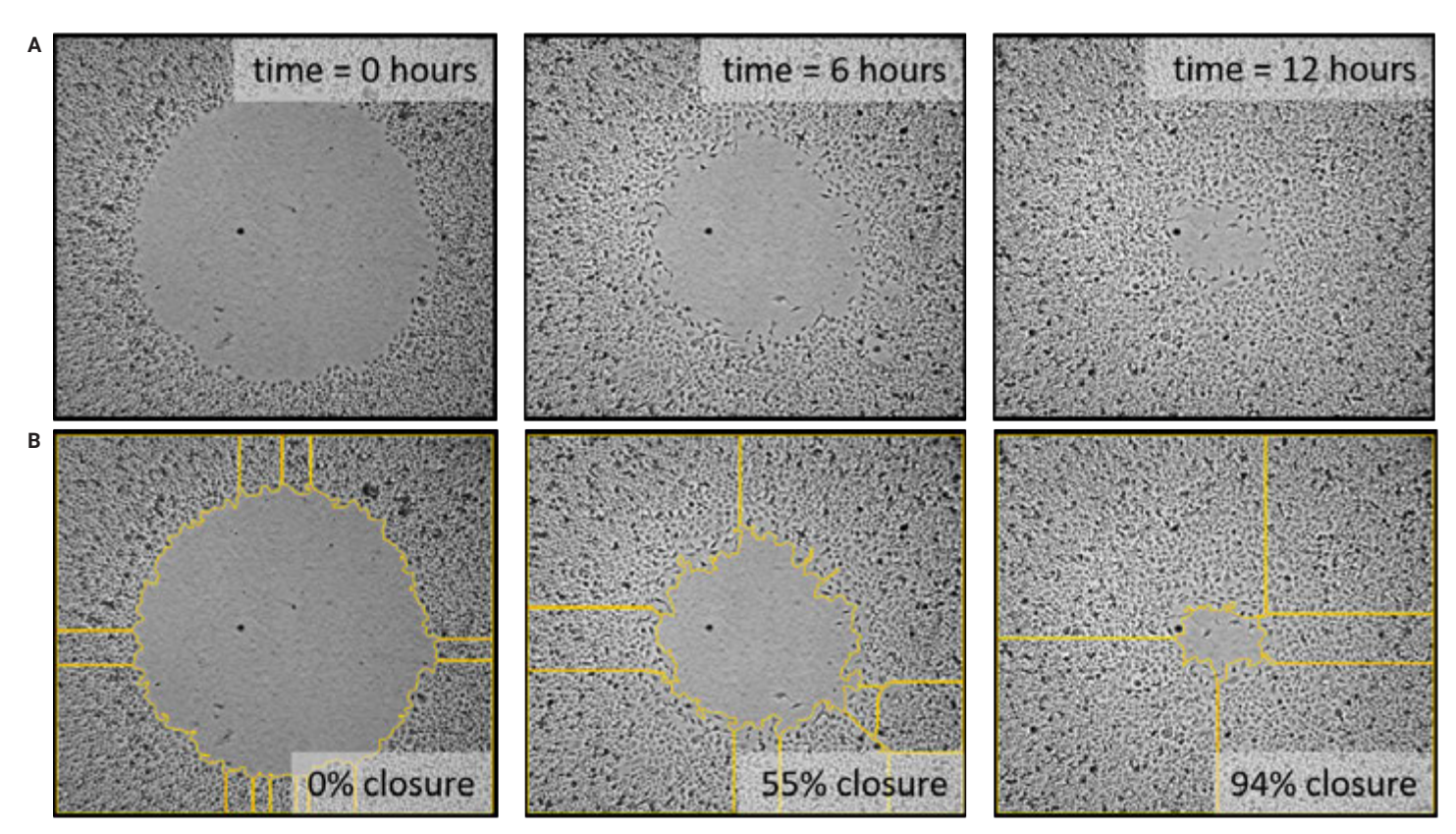
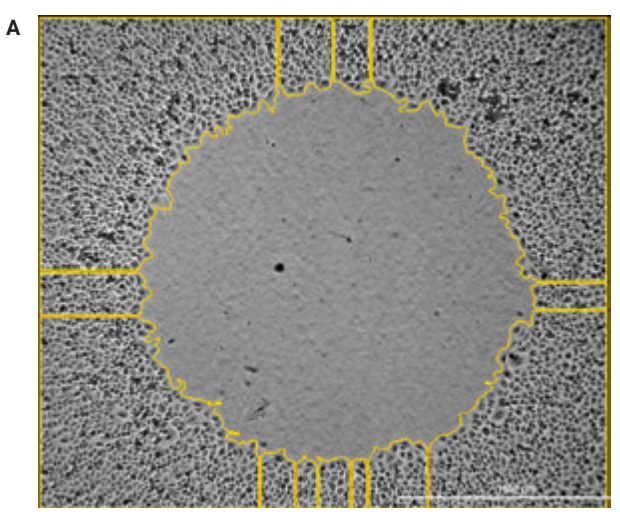
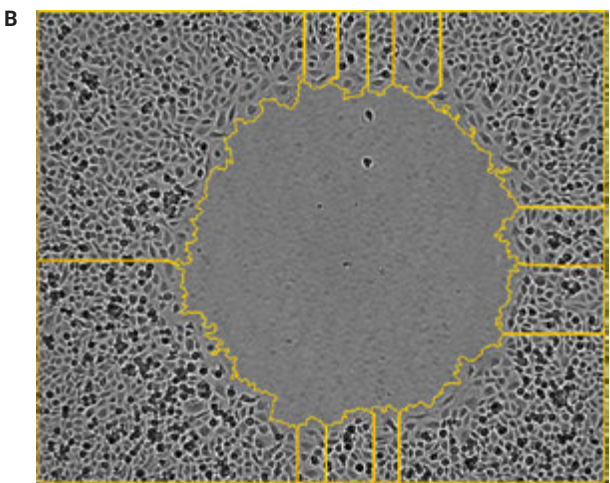


Figure 3. Uninhibited HT-1080 cell monitoring over time in 96-well microplates. Agilent BioTek Cytation 5 cell imaging multimode reader captured high contract brightfield images, 2.5x (A), and Agilent BioTek Gen5 microplate reader and imager software automatically placed object masks (yellow) over the total image area occupied by cells to calculate percent closure (B).

#### Comparison of 96-well and 384-well microplate formats

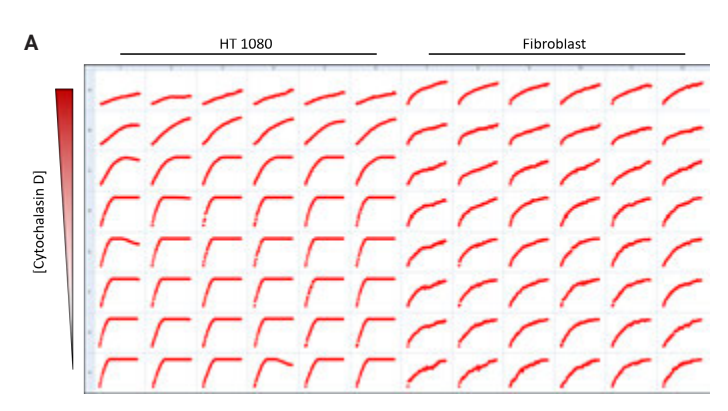
Kinetic imaging of the test plates was then compared using the collagen I coated 96-well and 394-well plate densities. Images were captured of HT-1080 cells, and object masks (Figure 4) were automatically placed around the cell-containing areas as previously described.





**Figure 4.** Image-based evaluation of HT-1080 cell migration characteristics in (A) 96-well microplate format using 2.5 objective; and (B) 384-well format using 4x objective. Yellow object masks were automatically placed over the total image area occupied by the cells.

The total image area occupied by the cells was used to calculate percent cell-free area closure for each well over the entire incubation period and in the presence of serially diluted inhibitor compound. Metrics for each plate and cell type were plotted versus time (Figure 5) to assess data consistency by comparing the kinetic curves from each well. The smaller size of the initial open areas in the 384-well plates resulted in slightly faster rates of closure than those observed in the 96-well format, yet both plate densities generated highly consistent results across replicates.



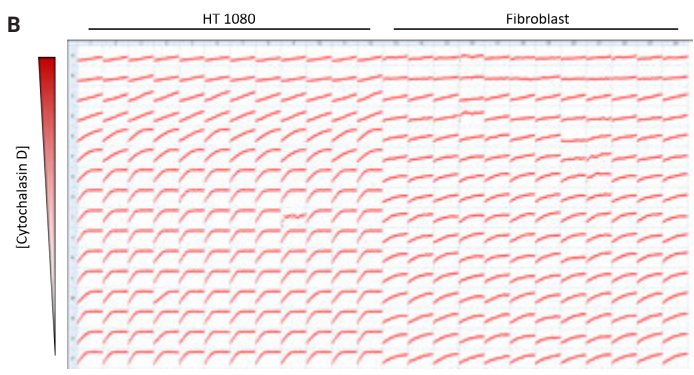


**Figure 5.** Full plate screenshots of plotted kinetic percent closure data. (A) 96-well plate with HT-1080 (left) and fibroblasts (right) cultured in the presence of serially diluted cytochalasin D. (B) 384-well plate with HT-1080 (left) and fibroblasts (right) cultured in the presence of serially diluted cytochalasin D. Both microplate densities generated highly consistent results across replicates.

Average kinetic curves from HT-1080 cells cultured in the presence of each cytochalasin D concentration were then plotted on a single graph for cells cultured in 96-well and 384-well microplate format (Figures 6A and 6B). Additionally, IC $_{50}$  values were calculated from the area under the curve (AUC) of the kinetic profiles. Data generated from both plate densities were nearly identical across replicates.

## Evaluation of cell health, morphology, and assay robustness

Detailed high-resolution images captured by Cytation 5 also enable qualitative evaluation of cell health and morphology during the experimental procedure to further characterize treatment effects. Per Figure 7A, fibroblasts treated with 37 nM cytochalasin D had significantly inhibited migration rates on the collagen I plates compared to untreated fibroblast cells without appreciable changes in morphology. In contrast, fibroblasts treated with 330 nM cytochalasin D exhibited altered morphology and apparent cell death. This information may be used in combination with quantitative results (Figures 7B and 7C) to further evaluate treatment effects.

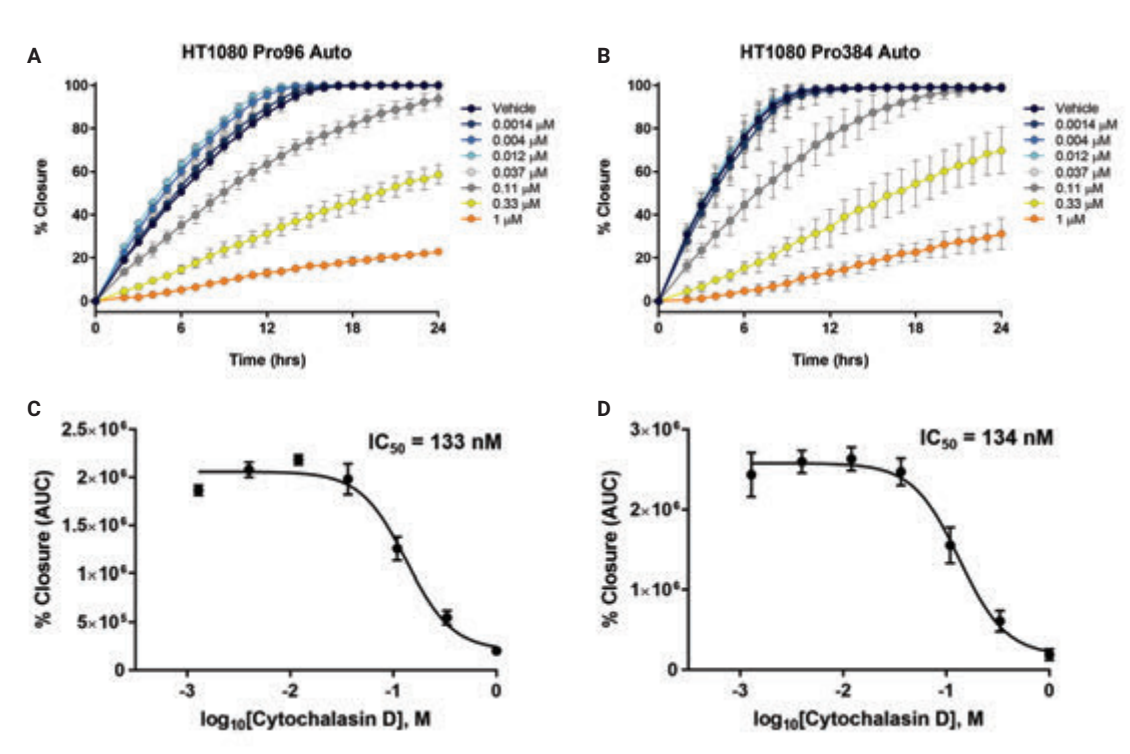


**Figure 6.** HT-1080 cytochalasin D dose response graphs. Average kinetic area closure including standard deviation for each cytochalasin D concentration at every captured timepoint in (A) 96-well format; and (B) 384-well format. AUC and  $IC_{50}$  values for each cytochalasin concentration after 12 hours in (C) 96-well format; and (D) 384-well format. Both microplate densities generated highly consistent results, including percent closure rates, AUD and  $IC_{50}$  values across replicates.

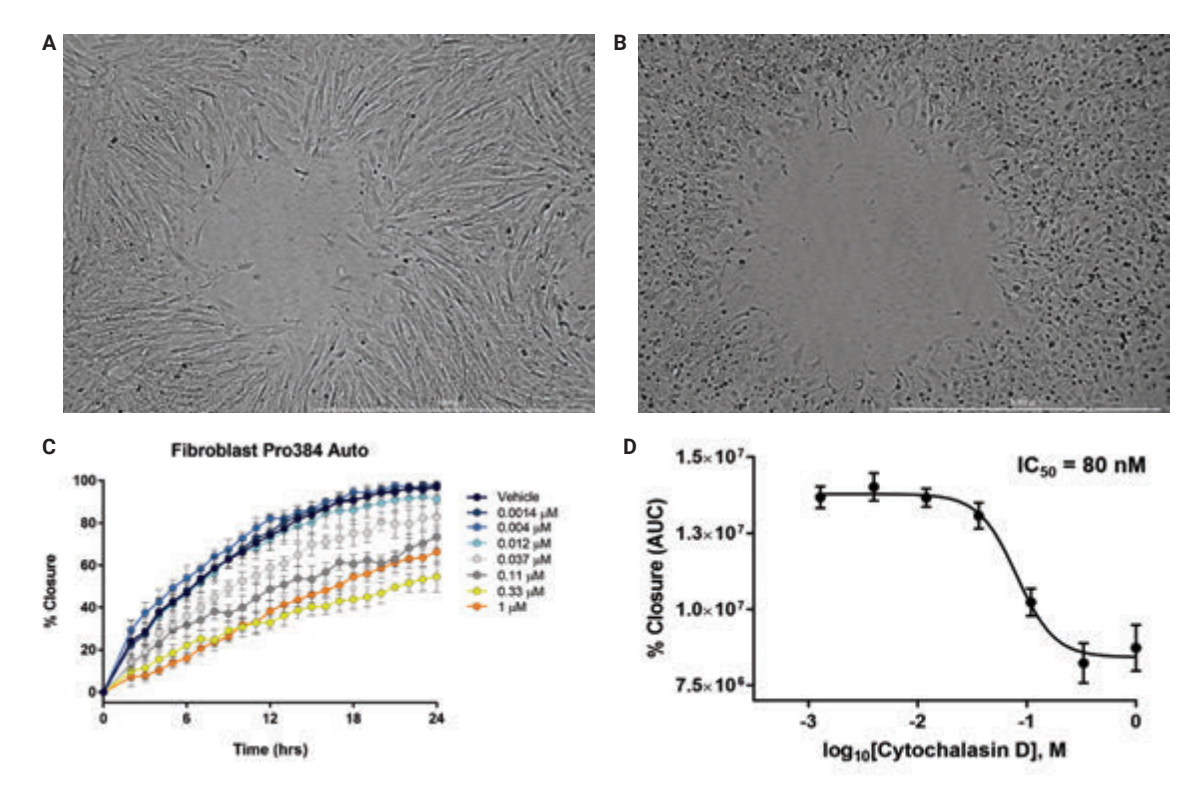


**Figure 7.** Qualitative and quantitative data on fibroblasts cultured in the presence of a serial cytochalasin D titration. High contrast brightfield images, 2.5x captured at 10 hours of fibroblasts exposed to (A)  $0.037 \,\mu\text{M}$ ; and (B)  $0.33 \,\mu\text{M}$  cytochalasin D. Cells treated with the higher inhibitor concentration exhibit altered morphology and apparent cell death. (C) Average kinetic area closure including standard deviation for fibroblasts cultured in the presence of each cytochalasin D concentration. (D) AUC and  $IC_{50}$  value for the cytochalasin titration after 10 hours.

Assay robustness in the high-throughput format was confirmed through Z' value calculations using HT-1080 cells treated with 1  $\mu$ M cytochalasin D as a positive control, and untreated cells as a negative control after 12 hours of incubation. Reproducibility of results and the large assay window achieved with this system resulted in a Z' value of

0.84 for the 384-well assay format (Figure 8A), and 0.81 for the 96-well format (data not shown). To demonstrate assay efficiency within a short period of time, Z' values relative to time were reported up to 12 hours. It can be observed that within 4 hours of starting the assay, a high Z' value of 0.56 was achieved (Figure 8B).

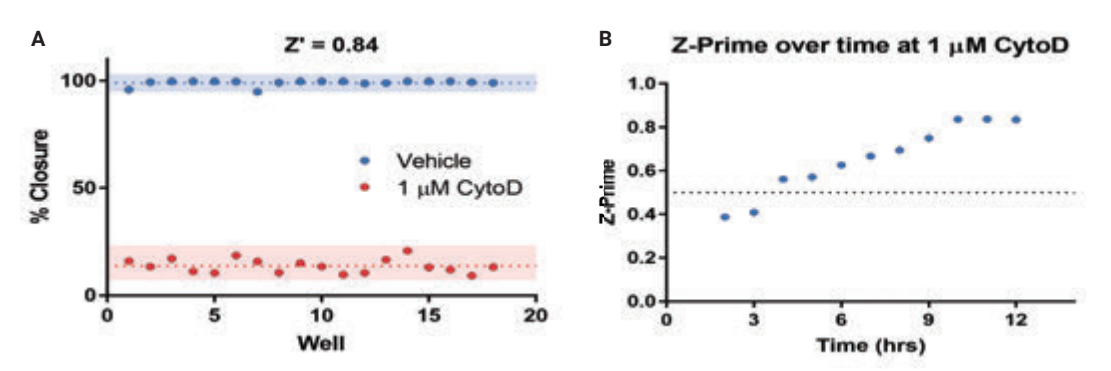


Figure 8. Comparison of results from HT-1080 cells exposed to 1  $\mu$ M cytochalasin (positive control, blue) to untreated cells (negative control, red). High Z' values indicate reproducible results in the automated assay format.

### Comparison of Oris technologies

The automated kinetic imaging workflow and image analysis described above can also be used with the Oris Cell Migration Assay platform that uses removable "stopper" barriers (Figure 9A). This format is only available in a 96-well plate and is not amenable to automated cell seeding, as the barriers require manual removal. However, the removable barriers provide the flexibility to treat the wells with any desired coating prior to running the assay. Images and resulting analysis generated using this format (Figure 9B) are comparable to those captured under the same conditions using the Oris Pro Cell Migration Assay protocol. Additionally, a kinetic cell migration profile of HT-1080 cells cultured in the presence of each cytochalasin D concentration on noncoated plates was plotted on a single graph (Figure 9C).

#### Conclusion

The label-free, fully automated Oris cell exclusion method provides a convenient solution for measuring cell migration. Automated liquid handling steps increase efficiency and improve assay results, while the Agilent BioTek BioSpa provided proper environmental conditions throughout the experimental procedure and enabled a walkaway workflow when coupled with Agilent BioTek Cytation 5. Cytation 5 with Gen5 image analysis software delivers reproducible quantitative results using both the 96- and 384-well microplate formats, while capturing a detailed qualitative record of cell morphology. The combined system produced high Z' values for high-throughput screening applications.

## References

- 1. Pollard, T. D.; Borisy, G. G. Cellular Motility Driven by Assembly and Disassembly of Actin Filaments. *Cell* **2003**, *112(4)*, 453–465.
- 2. Hanahan, D.; Weinberg, R. A. The Hallmarks of Cancer. *Cell* **2000**, *100*(*1*), 57–70.
- 3. Greenwood, J. et al. Lovastatin Inhibits Brain Endothelial Cell Rho-Mediated Lymphocyte Migration and Attenuates Experimental Autoimmune Encephalomyelitis. FASEB J. **2003**, 17(8).
- 4. Evsyukova, I.; Plestant, C.; Anton, E.S. Integrative

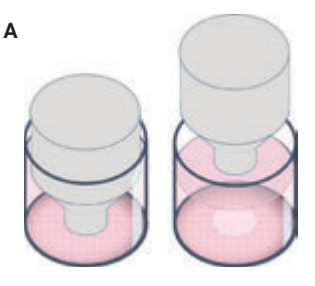
#### www.agilent.com/lifesciences/biotek

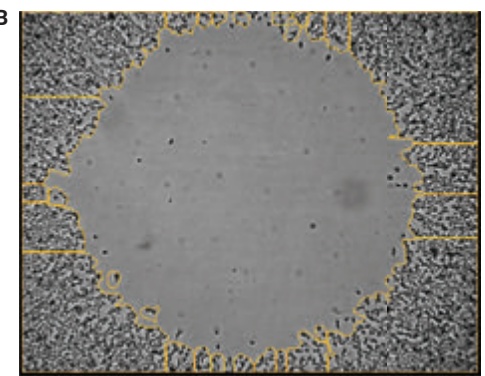
For Research Use Only. Not for use in diagnostic procedures.

RA44174.2307291667

This information is subject to change without notice.

© Agilent Technologies, Inc. 2019, 2021 Printed in the USA, April 1, 2021 5994-2583EN AN052019\_06





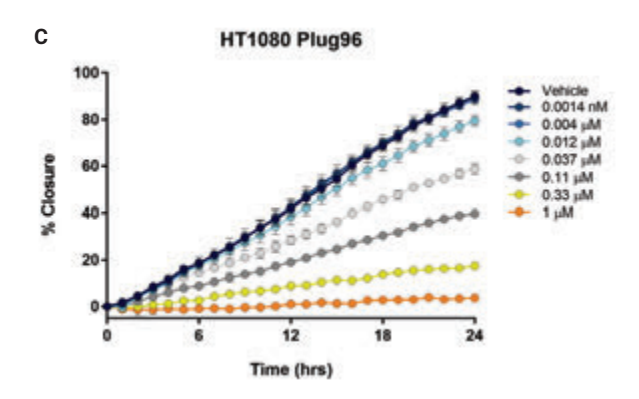


**Figure 9.** (A) Oris Cell Migration Assay stopper barriers. (B) Image of untreated HT-1080 cells cultured in 96-well format, 2.5x. (C) Kinetic cell migration profile of compound-treated HT-1080 cells cultured on a noncoated 96-well plate.

Mechanisms of Oriented Neuronal Migration in the Developing Brain. *Annu. Rev. Cell Dev. Biol.* **2013**, 29, 299–353.

